Eco-Friendly Cost-Effective Formation of Copper Oxide Nanostructures and its Prodigious Potential for Environmental Remediation Applications

Arun Thangadurai A.[1] and Sreenivasan V.S.[2,*]

[1]Assistant Professor, Department of Mechanical Engineering, VV College of Engineering, Tisaiyanvilai, Tamil Nadu, India.
[2]Associate Professor, Department of Mechanical Engineering, Sri Krishna College of Technology, Coimbatore, Tamil Nadu. India.
*to whom all correspondence should be addressed: e-mail: vssreenivasan@ymail.com

GRAPHICAL ABSTRACT

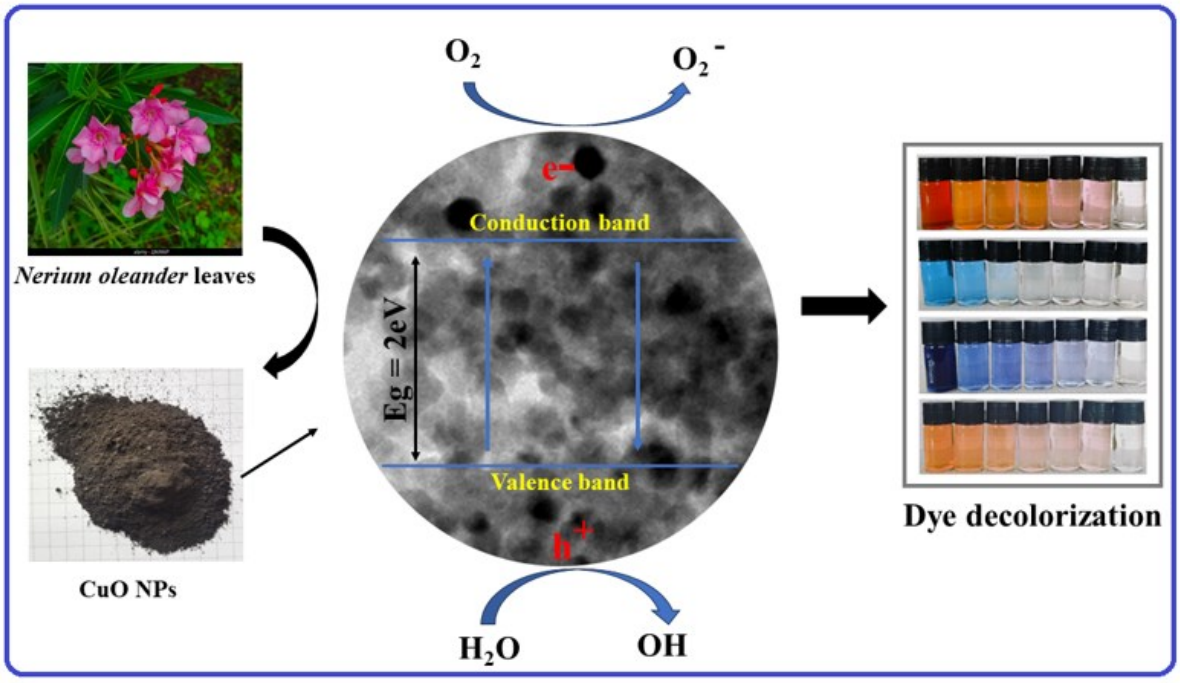

Abstract

The proliferation of environmental pollution, particularly from hazardous industrial dyes, poses a significant threat to ecosystems and aquatic life. This study uses extract from *Nerium oleander* leaves as a natural capping and reducing agent to produce copper oxide nanoparticles (CuO NPs), an ecologically acceptable way to tackle this problem. The CuO nanoparticles have improved physicochemical characteristics, as shown by their average crystalline size of 15.56 nm and decreased particle size of 31.84 nm. Additional studies such as SEM, EDX, TEM, and zeta

potential were accomplished and revealed the spherical structure; an elevated negative zeta potential of -25.6 mV was observed on the surface property. The photodegradation efficacy of these bio-synthesized CuO NPs was assessed against various industrial dyes, including Rhodamine 6G, Malachite Green, Eosin Yellow, and Reactive Black. The results demonstrated exceptional degradation efficiencies, with rates of up to 97.48%, 99.54%, 89.73%, and 89.33% respectively. The decolorization of organic dyes presented a visual cue that the degradation process was progressing. Notably, using Nerium oleander leaves as reducing agents contributed to the nanoparticles' stability, making them suitable for repeated cycles of photocatalysis. This research underscores the potential of green synthesis methods and highlights the vital role of plant-based reducing agents in advancing environmentally friendly nanomaterials for wastewater treatment and environmental remediation. The findings offer a promising pathway toward sustainable and eco-friendly solutions to mitigate the environmental impact of hazardous industrial dyes, fostering responsible industrial practices and preserving aquatic ecosystems.

Keywords: Copper oxide nanoparticles, *Nerium oleander* leaf, Enhanced physicochemical properties, Industrial dyes, Photocatalysis, and Decolorization.

1. Introduction

The rapid industrialization and urbanization of modern society have led to an alarming increase in environmental pollution. One of the most pressing challenges emanating from these transformative changes is the proliferation of environmental pollution, particularly organic dyes, which positions a significant threat to the ecosystem (Pakhale *et al.,* 2021). Rather than the more conventional natural coloring agents, hazardous dyes are usually exploited in the paper, leather, food, textile, printing, paints, cosmetics, and plastics sectors because of the significant financial, time, and labor commitment. Their presence in industrial wastewater has necessitated extensive and costly treatment processes, further straining limited resources. Moreover, releasing these dyes into natural water bodies disrupts the aquatic ecosystems, affecting the delicate balance of flora and fauna. The consequences of dye pollution include reduced water quality, oxygen depletion, and the endangerment of marine species (Al-Tohamy *et al.,* 2022). As a result, there is a pressing need to provide safe and ecologically suitable substitutes for these dangerous dyes to promote the shift to more conscientious and environmentally friendly industrial processes. One of the primary

categories of contaminants found in wastewater is organic dyes, and photocatalysts have been used extensively to disintegrate them into simple and less harmful or even non-toxic chemicals, reducing the potential damage that organic dye impurities cause to the environment and individuals (Berradi *et al.,* 2019). Besides, photocatalytic is a simple, scalable, and precise process to operate in a large-scale manner. It does not require following any challenging procedures to eliminate complex organic hazardous pollutants and make it suitable for industrial applications. Unlike other advanced treatment methods, photocatalysis does not involve intricate and resource-intensive processes. It is an attractive option for industries seeking eco-friendly, cost-effective solutions to tackle organic dye pollution (Kumari *et al.,* 2023).

Many prior research endeavors have unveiled the extraordinary versatility of copper oxide nanoparticles, establishing them as frontrunners in diverse scientific applications in electronics, sensors, energy storage, biomedicine, and catalysis (Kuspanov *et al.,* 2023). When combined with modern technology, copper oxide nanoparticles have attracted owing to their mechanical and biological characteristics compared to other metal nanoparticles (Udayabhanu *et al.,* 2015). Its distinctive characteristics, stability, low toxicity, and ability to generate reactive oxygen species under light irradiation make it an attractive choice for photocatalytic processes to mitigate the environmental impact of organic dyes. Their low toxicity, ecological compatibility, and cost-effectiveness align seamlessly with the burgeoning emphasis on sustainable practices, reinforcing their position as catalysts for responsible scientific solutions. The photocatalytic properties of nanomaterials are closely linked to their size and surface area. Smaller nanoparticles possess larger surface areas, leading to more active sites for photocatalytic reactions. These smaller particles absorb a broader range of light, exhibit faster charge carrier mobility, and may exhibit unique quantum size effects, all contributing to enhanced photocatalytic efficiency. From the benchmark studies, these properties could be optimized to advance the photocatalytic performance of the nanomaterial.

There are various physio-chemical methods of preparing nanomaterial using toxic reagents, complex organic solvents, hazardous stabilizing agents, and the involvement of expensive equipment accompanied by tedious experimental procedures (Sorbiun *et al.,* 2018). Nanomaterials are exceptional in their surface parameters; adhesion of any of the reagents on the surface of the nanomaterial would drastically affect the potential of the nanomaterial. Due to high energy requirements and low scalability, the physical preparation method is unsuitable for the

industrial-scale production of nanomaterial designed explicitly for an identified application. Green nanomaterial synthesis has caught the interest of academics. It is being widely interpreted in various conditions because of its ease of use, affordability, stability, environmental friendliness, and—above all—the fact that it removes any shortages (Sebeia *et al.,* 2019). Because plant extracts are sustainable and eco-friendly, much interest has been in using them as green-reducing agents (Ghazzal *et al.,* 2012). *Nerium oleander* leaves have become an essential natural resource in this field, providing several benefits for producing copper oxide nanoparticles (CuO NPs). Numerous phytochemicals, including steroids, terpenoids, polyphenols, and flavonoids, are present in these leaves and can naturally reduce and cap (Alaton *et al.,* 2001). The green and ecologically friendly method for synthesizing CuO NPs is devised by using the reducing power of Nerium oleander leaf extracts. This approach not only reduces the practice of detrimental chemicals but also improves the stability and homogeneity of the nanomaterials. *Nerium oleander* leaves' inherent reducing agent qualities mark a substantial advancement in producing sustainable nanomaterials, with a wide range of possible applications from environmental remediation to catalysis. To evaluate the produced CuO NPs' photocatalytic effectiveness against industrial pollutants, the most prevalent and dangerous two-cationic and anionic dyes of each kind were investigated.

The cationic dyes, namely Rhodamine 6G and Malachite Green, are the two most commonly used dyes in the textile and other industries as a coloring agent, particularly in the textile industry due to their high water-soluble nature (Sadollahkhani *et al.,* 2014). The unreacted dye molecules mixed up with the environmental water bodies directly affect human and aquatic life. They act as a carcinogenic agent when entering the human body. The two most often used anionic dyes that impact marine life and create aesthetic issues are Reactive Black and Eosin Yellow. These dyes impede the flow of oxygen and light into water. Reactive black is a dye consumed extensively for reactive dying (Singh *et al.,* 2023).

2. Experimental Procedure

2.1 Chemicals Components

The Cupric Chloride Dihydrate [$CuCl_2$. $2H_2O$] (98%) (CAS 10125-13-0) was acquired from Loba Chemie Pvt. Ltd., a company based in Mumbai, India. The ethanol (C_2H_5OH) with a purity of 99.9% was obtained from Changshu Hongsheng Fine Chemical Co. Ltd., located in China. The

leaves of *Nerium oleander* were gathered from the roadsides of Tiruchengode, serving as the essential precursor materials acquired externally.

2.2 Preparation of Nerium Oleander Extract

Nerium oleander leaves were taken straight from the plants. Water and ethanol were used to wash the leaves until all the dust and dirt were eliminated. After proper cleaning, the leaves were shadow-dried and grounded. 100 ml of double-distilled water and 2 g of *Nerium oleander* leaf powder were stirred at 80°C for one hour, then left undisturbed overnight at room temperature. Later, the mixture underwent filtration with Whatman No. 1 filter paper. The resulting essence was termed the *Nerium oleander* leaf extract.

2.3 Preparation of CuO Nanoparticles

1 M of Copper chloride was added to 100 ml of prepared *Nerium oleander* leaf extract, which was placed under the magnetic stirrer at 50°C. The setup was undisturbed for 6 hours handset and set aside to rest overnight for proper nucleation growth. Then, the mixture was sonicated for 120 min at 40 Hz of power to ensure homogeneity and centrifuged thrice with water and ethanol each to separate the impurities over the nanomaterial. After that, the solution was dried in a hot air oven. The dried sample was grounded and calcined for three hours at 500°C. The material was granulated and placed in a container after it reached room temperature (Singh et al., 2023)

2.4 Characterization

The crystalline structure of the prepared nanoparticles, as well as their texture, were discovered by the use of an X-ray diffraction (XRD) investigation. A radiation source with a wavelength of Cu K was used to scan the sample at room temperature. Additionally, the Rietveld refinement technique was utilized to estimate the refinement parameter of CuO nanoparticles. The outcome was achieved by using Fullprof analytical software, which was endowed with the pseudo-Voigt function and employed linear interpolation between pre-established baseline points with adjustable height. Fourier transform infrared spectroscopy (FTIR-Spectrum 100; PerkinElmer, USA) was utilized to investigate the phytochemical makeup of the CuO nanoparticles and the functional groups they contain.

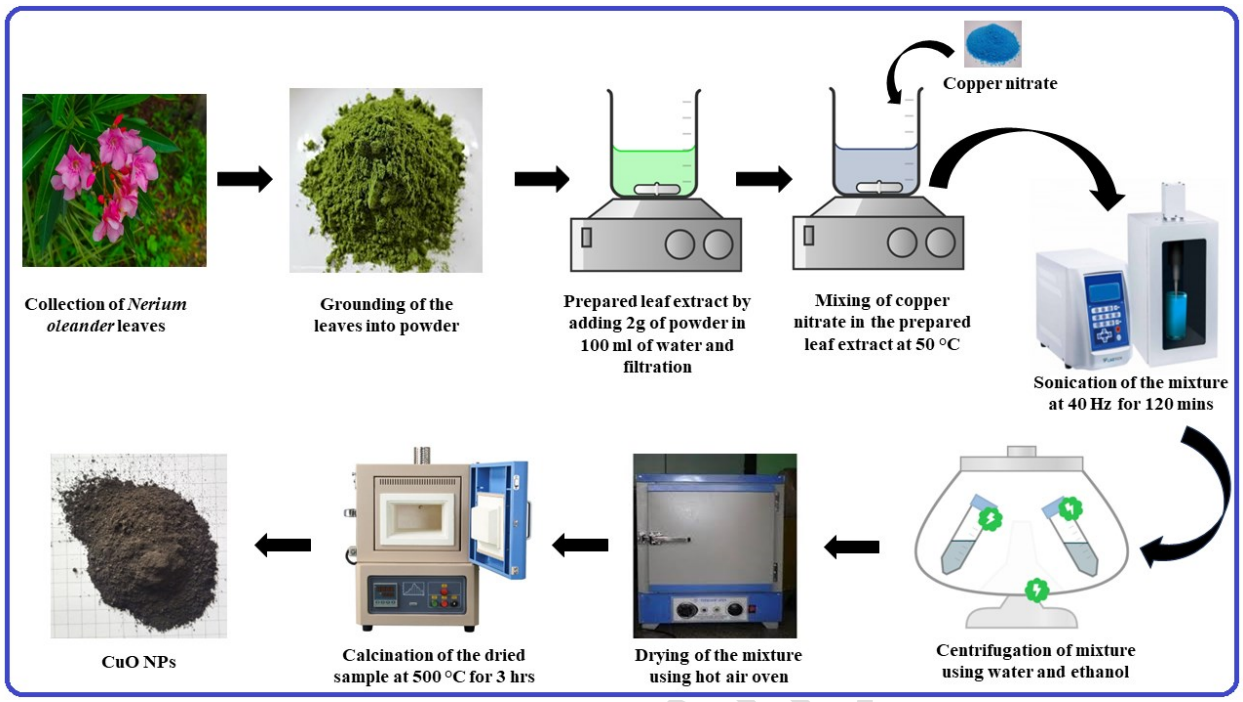

Figure 1. The schematic representation of CuO nanoparticle synthesis

We calculated the average particle size distribution using a Particle Size Analyzer (PSA; Nanophox, Sympatec, Germany). The influence of dynamic light scattering broadened the particle size distribution throughout a range of 1-100 nm and at a scattering angle of 90º.

The absorption and transmission properties of CuO nanoparticles were investigated using the UV-Vis spectrophotometer (Cary 8454 model, marketed by Agilent in Singapore). The analysis of the textural topography was conducted with a scanning electron microscope (SEM- SIGMA HV – Carl Zeiss with Bruker Quantax 200 – Z10 EDS Detector). Furthermore, the CuO nanoparticles synthesized were analyzed using transmission electron microscopy (TEM) and selected area electron diffraction (SAED) techniques to determine their crystalline structural features and lattice parameters.

2.5 Preparation of Reaction Mixture for Photocatalysis

Under sunlight, the destruction of anionic and cationic model industrial pollutants, namely Rhodamine 6G, Reactive Black, Eosin Yellow, and Malachite Green, was used to measure the photocatalytic effectiveness of the produced CuO NPs. The reaction mixture was prepared by adding 100 ppm of Organic dye to the distilled water. Upon that, 100 mg of prepared CuO NPs was added and placed on a magnetic stirrer for 30 minutes to attain homologous. The whole process was carried out in dark circumstances. Then, the setup was transferred to the sunlight to

facilitate the energy source. The time-dependent degradation of organic dye molecules was estimated by collecting 3 ml of the reaction mixture and examining it under UV-Vis spectroscopy every 15 minutes. The process and timely examination of the reaction mixture continued until the nanomaterial's maximum catalytic potential was achieved. The following Removal Percentage Equation (1) was used to compute the degradation effectiveness (%) of the CuO NPs (Singh *et al.,* 2023).

$$\eta = \left[\frac{C_0 - C_t}{C_0}\right] \times 100\ \% \qquad (1)$$

Where, η denotes the percentage of degradation, C_0 denotes the dye's initial absorbance, and C_t denotes the dye's change in absorbance over time.

3. Result and discussion

3.1 XRD

The XRD pattern of the CuO NPs from *Nerium oleander* leaf extract, depicted in Figure 2, shows its highly crystalline nature. The characteristic peaks were detected at 2θ angles of 32.41, 35.42, 38.69, 46.11, 48.69, 53.4, 58.13, 61.48, 66.01, 68.6 and 74.95 with respective miller indies of (110), (-111), (111), (-112), (-202), (020), (-113), (311), (220), (311) and (-222). By comparing the acquired data with the International Center of Diffraction Data files (ICDD), the production of highly crystalline CuO NPs was verified. The finding lines up with the JCPDS-80-1916 card, which reveals the monoclinic single-phase structure of the nanoparticles (Roisnel *et al.,* 2001). The lack of additional peaks exhibited the purity of the nanoparticles. The Scherrer formula shown in equation (2) was used to determine the average crystalline size of the created CuO NPs, which was 15.56 nm (Alaton *et al.,* 2001). The compact structure and reduced average crystalline size resulted from using *Nerium oleander* leaf extract as a reducing and stabilizing agent and perfect calcination temperature with adequate timing.

$$D = \frac{K\lambda}{\beta cos\theta} \qquad (2)$$

Where, D embodies the crystallite size of CuO NPs, K signifies the Scherrer constant (values from 0.9 to 1), β represents the diffraction peak's FWHM, λ stands for the wavelength (X-ray source 0.1541 nm used during XRD analysis), and θ represents the Bragg angle respectively.

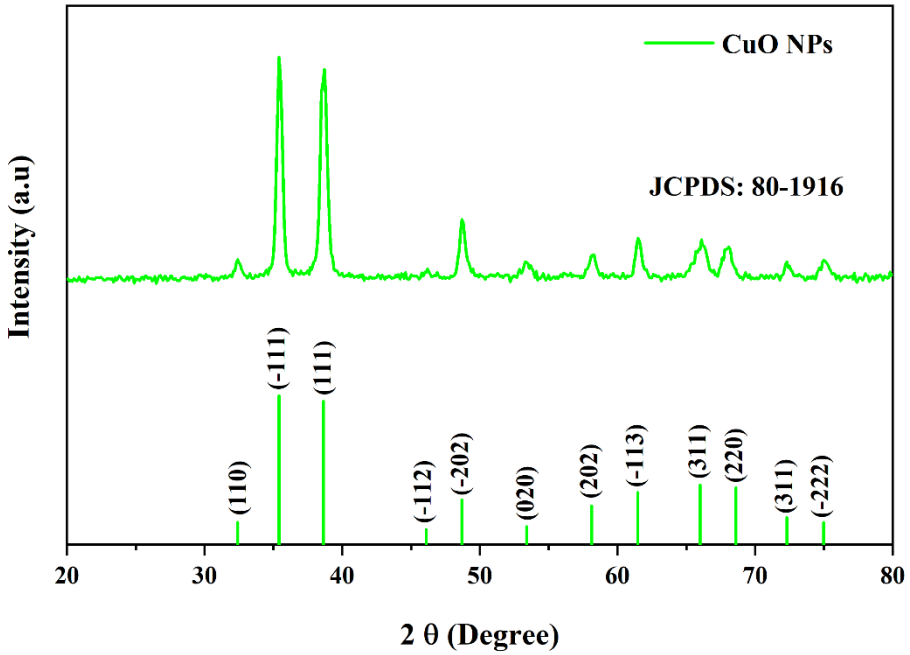

Figure 2. XRD pattern of prepared CuO NPs

The Rietveld Refinement technique determined the CuO NPs' structural properties (Sadollahkhani *et al.,* 2014). Figure 2 depicts the Rietveld Refinement of the prepared CuO NPs. The refined structural parameters are specified in Table 2. The refinement data yielded the lattice parameters of a, b, and c, which were 4.6830 Å, 3.4290 Å, and 5.1300 Å, respectively. The obtained good-to-fit values of the CuO NPs of the advanced graph align with the estimated and acquired data. These slight variations may be caused by the variation in the synthesis procedure and utilization of different capping and reducing agents and their volumes.

Table 1. Structural parameters of prepared CuO NPs

Miller indices	2 theta (degree)	FWHM (degree)	Crystal size (nm)	d-spacing (Å)	Dislocation density in 1/nm^2
(1 1 0)	32.4333	0.3897	21.29217	2.76054	0.002206
(1 1 -1)	35.4504	0.4871	17.03484	2.53221	0.003446
(1 1 1)	38.6424	0.5845	14.19641	2.33007	0.004962
(2 0 -2)	48.7375	0.3897	21.29217	1.86845	0.002206
(0 2 0)	53.4668	0.5845	14.19641	1.7138	0.004962
(2 0 2)	58.2239	0.5845	14.19641	1.5846	0.004962
(1 1 -3)	61.524	0.3897	21.29217	1.50729	0.002206
(3 1 -1)	66.2533	0.7793	10.64819	1.4107	0.00882

(2 2 0)	68.0501	0.6819	12.16888	1.37777	0.006753
(3 1 1)	72.3791	0.5845	14.19641	1.30566	0.004962
(0 0 4)	75.0353	0.7793	10.64819	1.26589	0.00882
		Average	**15.5602**		**0.00493**

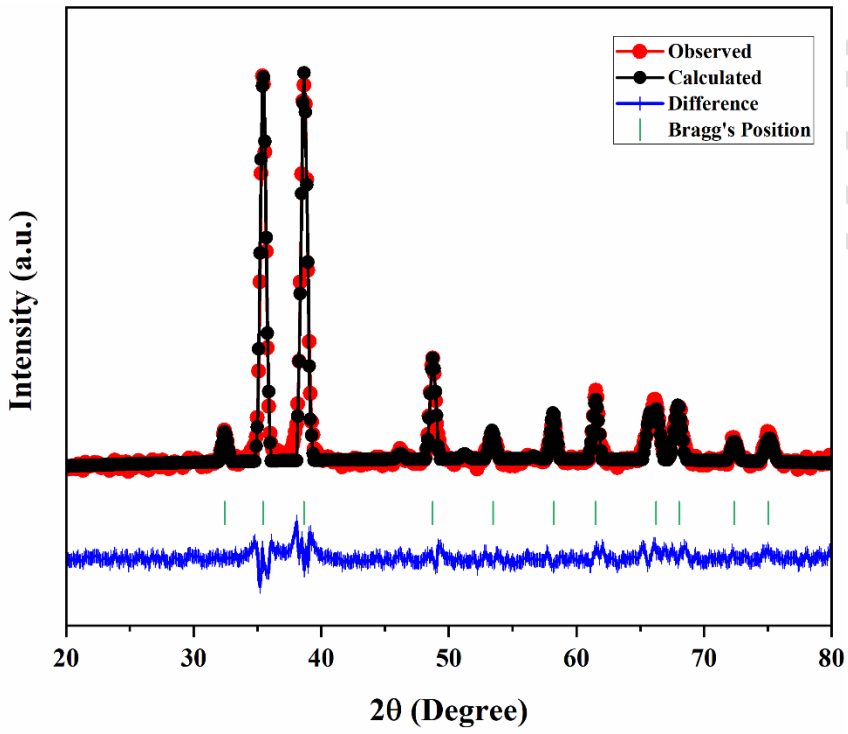

Figure 3. Rietveld Refinement pattern of prepared CuO NPs

Table 2. Rietveld Refinement parameters of the CuO NPs

Structure: Monoclinic			**Space Group:** C12/C1			**Space group number:** 15		
a (Å)	**b (Å)**	**c (Å)**	**Volume (Å)**	**R_p**	**R_{wp}**	**R_{exp}**	**χ^2**	**Crystallite Size (nm)**
4.6830	3.4290	5.1300	82.378	5.6568	7.6750	5.85273	1.7196	15.5602

3.2 Functional Group Analysis

The FTIR spectra of the CuO NPs are depicted in Figure 4. The CuO NPs' stretching vibration was linked to the stretching vibration mode at 462 and 637 cm^{-1} (Singh *et al.* 2023). This peak demonstrated the nanoparticles' structural makeup and confirmed the monoclinic phase of CuO NPs, as reported in the XRD study (Eskizeybek *et al.* 2012). The intense peak at 1384 cm^{-1} was

ascribed to the carbonyl group (C=O). The enormous peak can observe the hydroxyl group (O-H) stretching vibration at 3430, 3776, and 1635 cm^{-1}; these might result from the absorption of atmospheric water molecules by the CuO NPs (Chen *et al.* 2007).

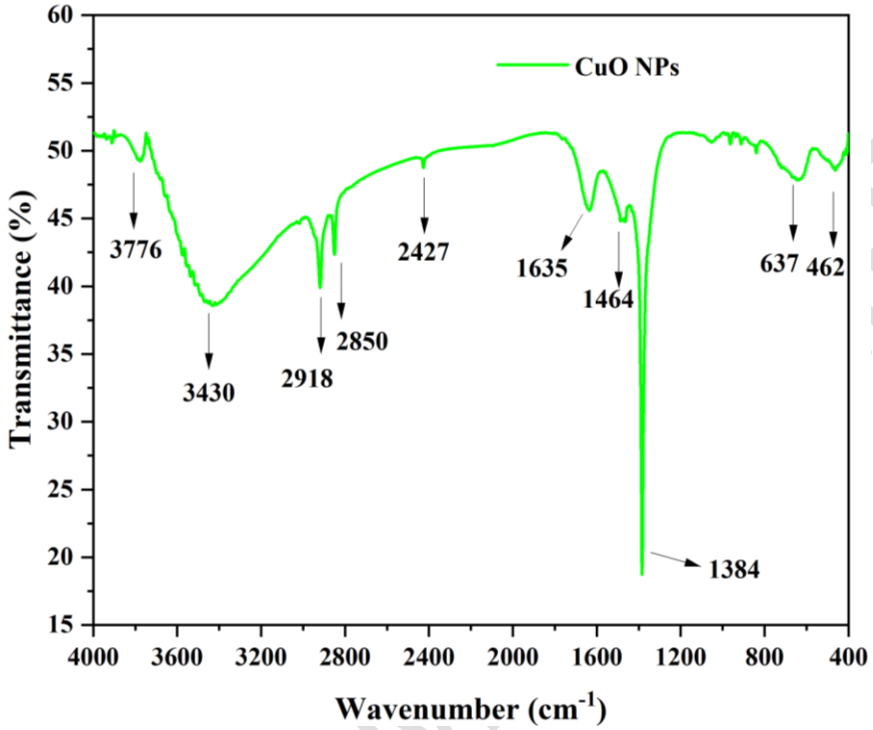

Figure 4. FT-IR spectrum of CuO NPs

The minute symmetrical vibration at 2427 cm^{-1} represents the existence of CO_2 that was added to surfaces from the atmosphere (Shirmardi *et al.* 2013). The absorption band at 2850 and 2918 cm^{-1} represents the stretching vibration of an alkyl functional group (C-H) (Bilal *et al.* 2018). The absorption band at 1464 cm^{-1} exhibits the aliphatic C–H group (Laohaprapanon *et al.* 2015). The absence of unnecessary peaks represents the lack of impurities in the prepared NPs.

3.3 Particle Size Analysis

Figure 5 represents the results of the dynamic light scattering (DLS) technique used to inspect the particle size of the produced CuO nanoparticles. Particle size analyzer findings revealed that the average particle size (d_{50}) of CuO NPs is 31.84 nm. The efficient capping and reducing characteristic of the *Nerium oleander* leaf extract was responsible for the complete decrease in the particle size of nanoparticles. The color of the nanomaterial depends on its size and structure due to its distinct optical properties. Generally, the copper oxide nanomaterial is in three color variants: black, brown, and reddish brown. The nanomaterials with larger particle sizes appear black, and

nanomaterials with smaller particle sizes tend to appear reddish or brown. The prepared CuO NPs appeared in a light reddish-brown color that visually represents the smaller particle size. The reduced particle size explains the effective surface property of the nanomaterial that would act as an effective photocatalytic agent.

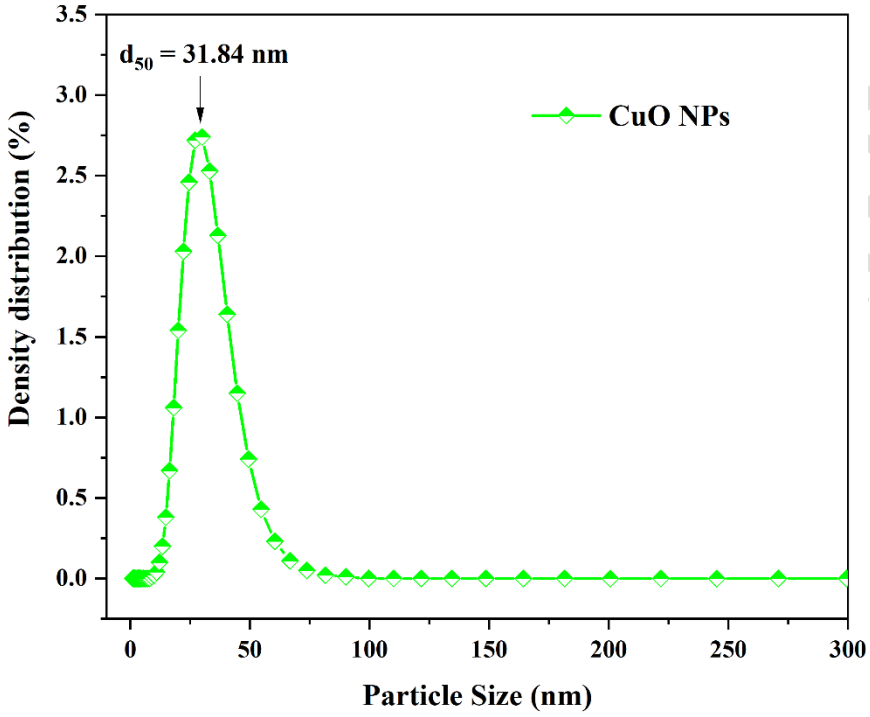

Figure 5. Particle Size Analysis of prepared CuO NPs

3.4 SEM and EDX analysis

The morphology and elemental composition of the CuO NPs are portrayed in Figure 6. From the outcomes, it was obvious that the nanoparticles were spherical with an agglomerated porous nature. The produced CuO NPs were homogeneous in the clustery structure and had a size in the nanometer range. With 20,000 X of magnification, it is evident that the porous nature of the nanomaterial seems to be a sponge-like structure. The porous and agglomerated nature of the nanoparticles provides an extensive surface area, ideal for increased reactant adsorption and reduced electron-hole recombination, extending the lifetime of charge carriers for more effective redox reactions.

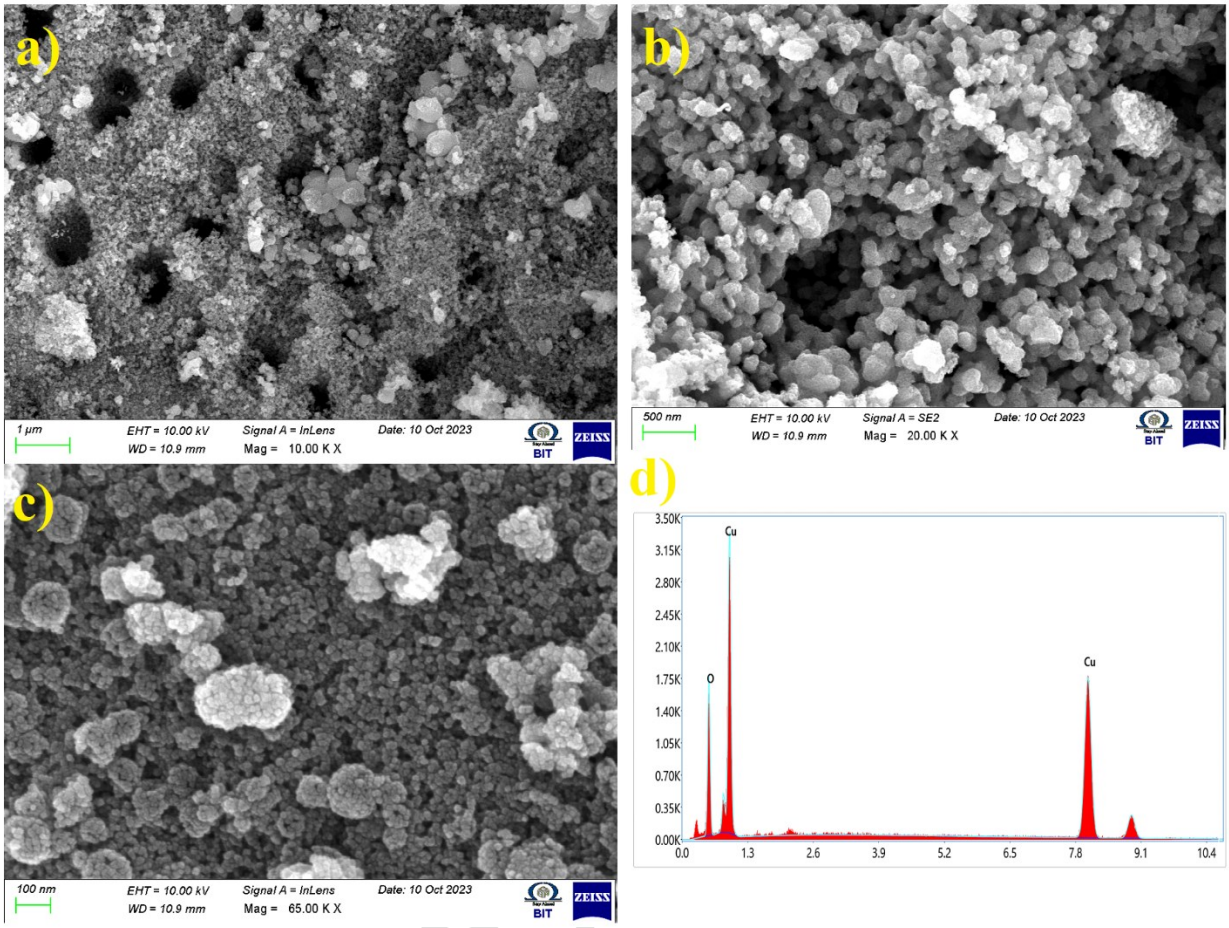

Figure 6. SEM images and EDAX of the prepared CuO NPs

The spherical shape and porous structure allow for efficient light penetration, leading to enhanced photon absorption and utilization in photocatalytic responses, and also permit easy separation for potential reusability. The remarkable reducing and capping abilities of the *Nerium oleander* leaf extract are worth mentioning, as they led to the creation of morphologically tailored nanoparticles. The lack of other elemental contaminations in the elemental composition study indicated the existence of pure CuO nanoparticles. The intensity of the peaks represents the elemental concentration of Cu and O in the sample. The ratio of the elements was estimated to be 56.3 and 43.7 for the Cu and O, respectively.

3.5 TEM and SEAD analysis

Figure 7 represents the results of Selected Area Electron Diffraction (SAED) and Transmission Electron Microscopy (TEM) on the produced CuO NPs.

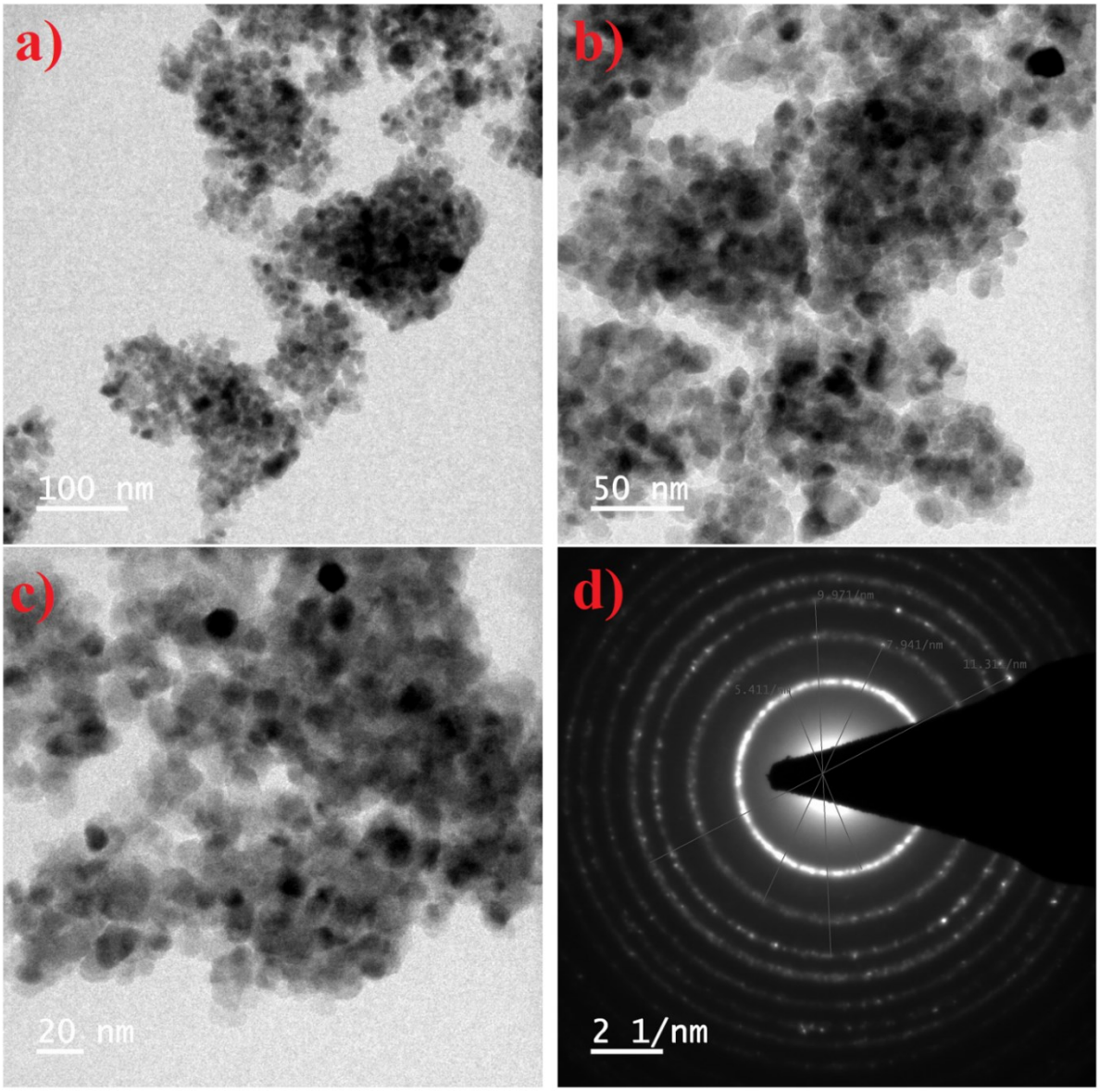

Figure 7. TEM and SAED pictures of the CuO NPs

The smooth and spherical nature of the NPs with a narrow size distribution in the nanometer range was evident from the results. The produced CuO NPs were shown to be crystalline by the SAED analysis. Diverse diffraction rings of monoclinic CuO were seen in SAED patterns. The spots in the rings align with the respective plane findings from the XRD analysis. These outcomes underpin the results derived from the XRD analysis, Particle size analysis, and SEM analysis of the prepared NPs.

3.6 UV–Vis Spectroscopy Study

The UV-Vis spectrum of absorption and direct bandgap was depicted in Figure 8 and 9. The distinctive peak at 363 nm represents the characteristic peak of CuO NPs, which indicates a redshift in the absorption wavelength (Lucas *et al.* 2006). This redshift could provide valuable insights into the structural and electronic properties of the nanomaterial. The redshift in the absorption peak reveals that the CuO NPs possess unique size and shape-dependent properties. In nanomaterials, such shifts in absorption peaks could be attributed to quantum confinement effects. When the size of nanoparticles decreases, the electronic structure is modified, leading to altered absorption properties. In the case of CuO NPs, a redshift typically indicates that the nanoparticles are smaller than their bulk counterparts, resulting in a widening of the bandgap. The results from XRD and particle size analysis also align with the findings that add more evidence to the crystalline nature of the produced NPs.

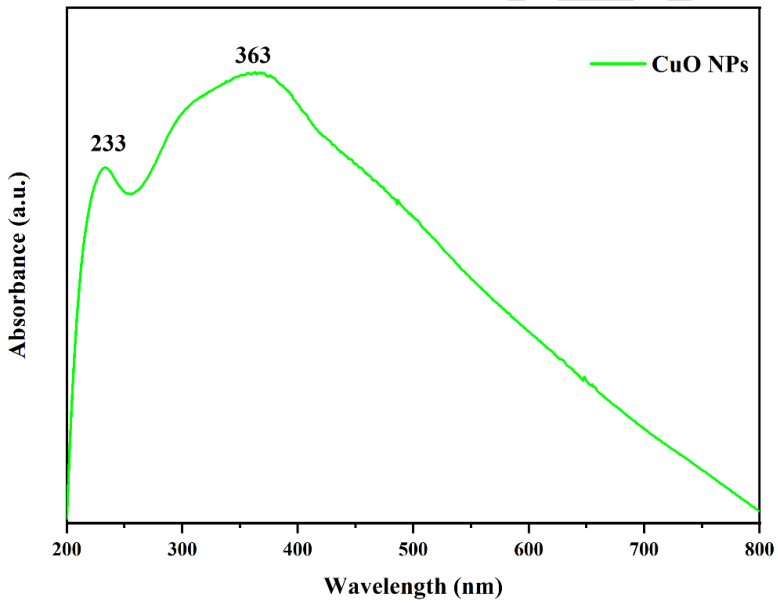

Figure 8. UV-visible absorption spectrum of CuO NPs

The bandgap of CuO NPs was estimated by plotting the CuO NPs Transmittance graph and Tauc's plot equation (Equ.3), as illustrated in Figure 9.

$$(\alpha h\nu)^{1/2} = A(h\nu - Eg) \qquad (3)$$

Wherem α is the representation of the absorption coefficient, h is the representation of the Planck constant, ν is the representation of the frequency of the incident light, A is the representation of the proportionality constant, and Eg is the representation of the bandgap energy. The direct bandgap of the produced nanoparticles was determined by obtaining a graph between $(\alpha h\nu)^{1/2}$ Vs. hν, as revealed in Figure 8. The direct bandgap of created nanoparticles was estimated at 2.1 eV.

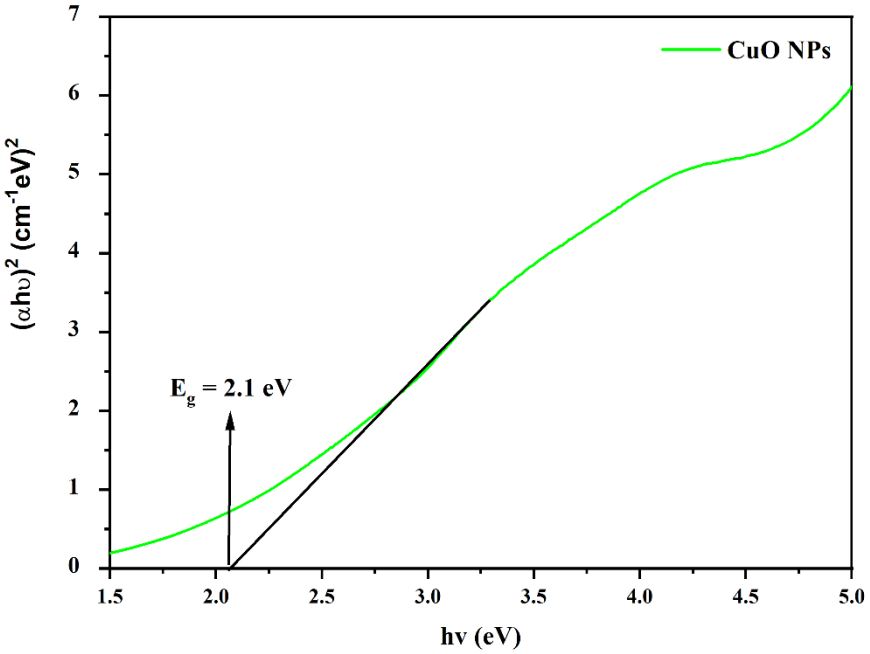

Figure 9. Direct band gap of CuO NPs

3.7 Zeta Potential Analysis

Figure 10 illustrates the results of the Zeta potential study of the produced nanoparticles. The nanoparticle's stability, electrophoretic nature, surface charge, and dispersion behavior were visually determined from the obtained results. The Zeta potential of the prepared nanoparticles was estimated at -25.6 mV. Generally, nanomaterials having greater than +30 mV or lesser than -30 mV of zeta potential are highly stable materials (Singh *et al.* 2019). The electrostatic repulsive force (surface charge) and stability of the nanomaterial are directly proportional if the electrostatic repulsive force is positive and inversely proportional if it is negative. While the nanoparticle is dispersed in a dispersion medium based on the strength of electrostatic repulsion between the nanoparticles, the particles become stable. A more vital repulsive force exists between the nanoparticles as their zeta potential shows a substantial negative value. This prevents the aggregation of nanoparticles in the medium and results in long-term stability. The nanoparticle produced from Nerium oleander leaf extract was 4.57 times more potent than copper oxide nanomaterial made by a conventional chemical method (Laohaprapanon *et al.* 2015).

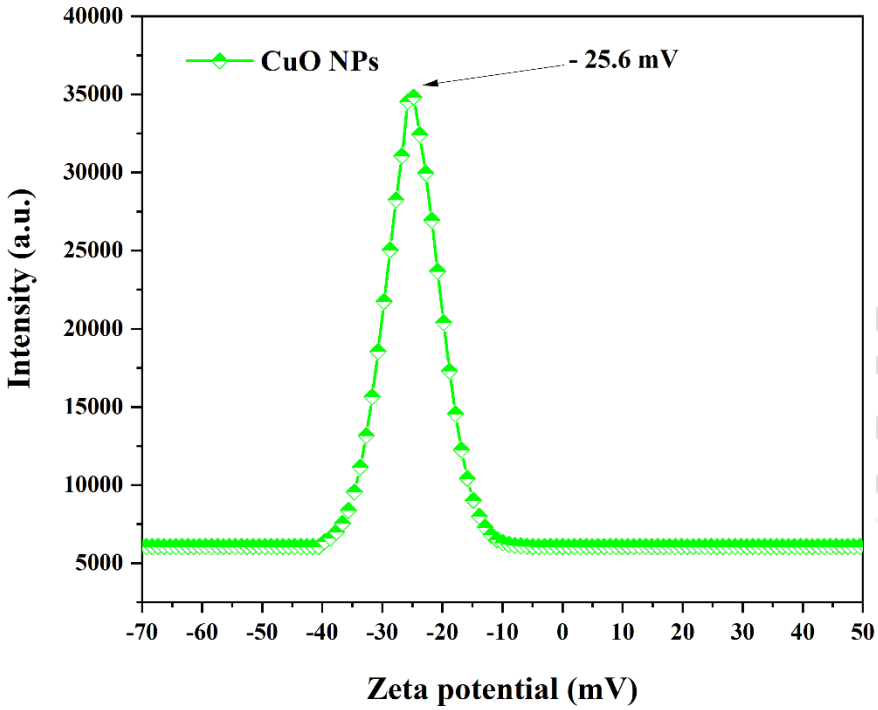

Figure 10. Zeta Potential of prepared CuO NPs

3.8 Photocatalytic Efficacy of CuO NPs

The efficacy of prepared NPs from *Nerium oleander* leaf extract in photocatalytic degradation of cationic dyes, namely Rhodamine 6G and Malachite Green, is illustrated in Figures 11(a, b) and 12 (a, b). The whole process was demonstrated in the middle of the day so that the process would be facilitated with the fullest wavelength potential of the sun. Under dark circumstances, to attain homogeneity, the reaction mixtures were stirred for 30 min before exposing the reaction mixtures to the sunlight. Then, the whole setup was transferred to the open sunlight. The mixtures were examined under UV-Vis spectroscopy at regular intervals of 15 minutes to assess the efficacy of the nanomaterial and time-dependent degradation of organic dye material. The characteristic peaks of Rhodamine 6G and Malachite Green were observed at 528 nm and 618 nm, respectively (Laohaprapanon *et al.* 2015). The timely degradation of dye molecules against the CuO NPs was observed in the graphic collected every 15 minutes. The maximum degradation of both dyes was observed subsequently 90 minutes. The efficacy of the CuO NPs against anionic dyes such as Rhodamine 6G and Malachite Green was 97.48% and 99.15 %, respectively.

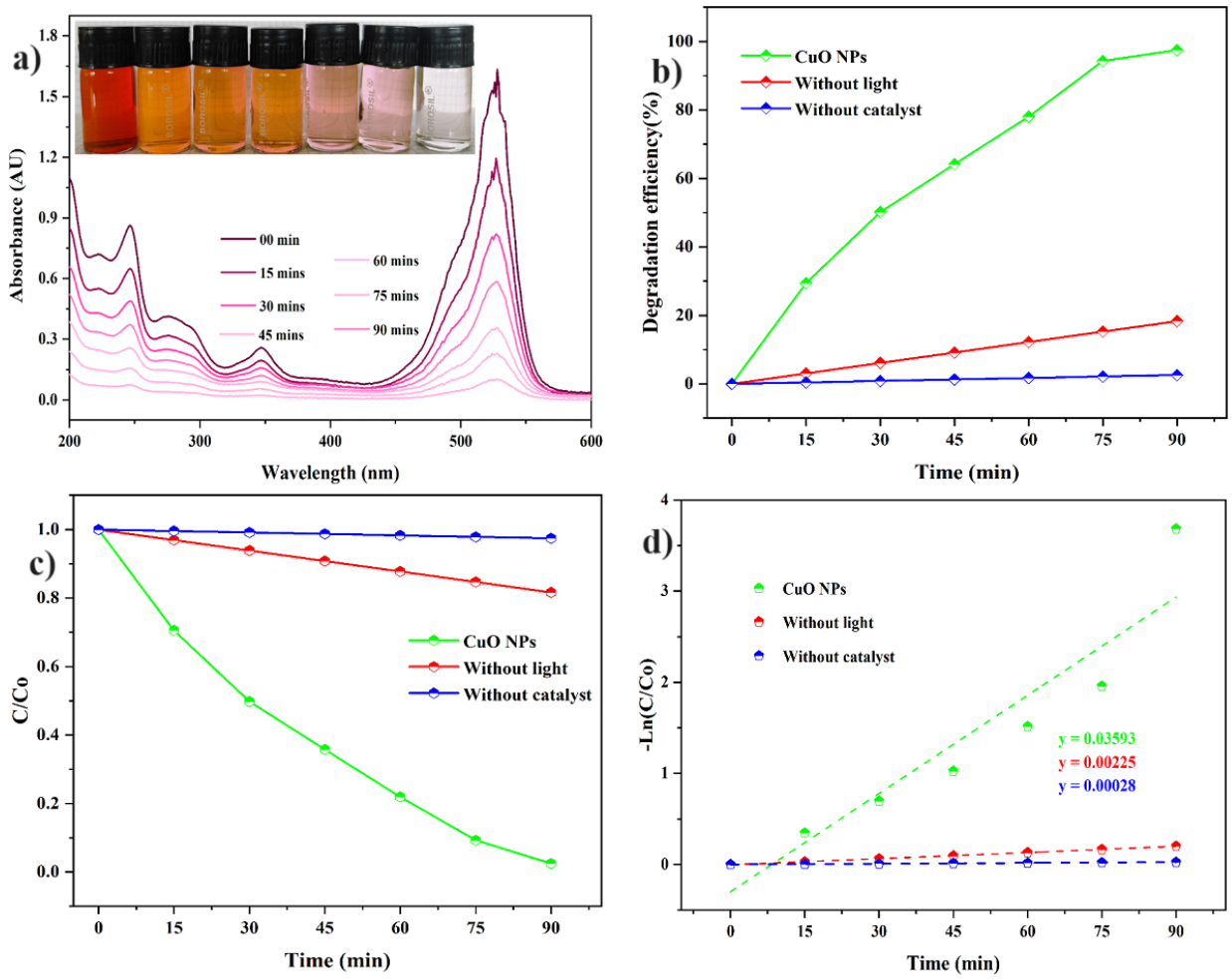

Figure 11. Photocatalytic degradation, efficiency, C_t/C_0 curve concerning time and Pseudo first-order kinetics of the CuO NPs against Rhodamine 6G Dye

Separate solutions were prepared for Rhodamine 6G and Malachite Green without adding CuO NPs as a catalyst to evaluate the self-degradation of anionic dyes in the occurrence of sunshine. Thus, the self-degradation of the dye molecules by the natural factors can be evolved. These solutions served as control groups. The reaction mixture was exposed to sunlight after being stirred for half an hour, as in the previous protocol. Utilizing UV-Vis spectroscopy, the self-degradation of the organic dye molecules was tracked over time by the decalin of the distinctive peaks at regular intervals of 15 minutes. At the end of 90 minutes, 2.57 % and 2.23% of Rhodamine 6G and Malachite Green dyes were self-degraded, which was negligible compared to the degradation efficacy of the process done with the catalyst. To access the light-dependent catalytic activity of the nanomaterial, the procedure was repetitive with the presence of the catalyst under dark circumstances. In this way, the decomposition of the organic dye molecules by the catalytic

potential of the nanomaterial can be evolved. At the end of the same time, the nanoparticles revealed a degradation efficacy of 18.36% and 17.86% for the Rhodamine 6G and Malachite Green dyes, respectively.

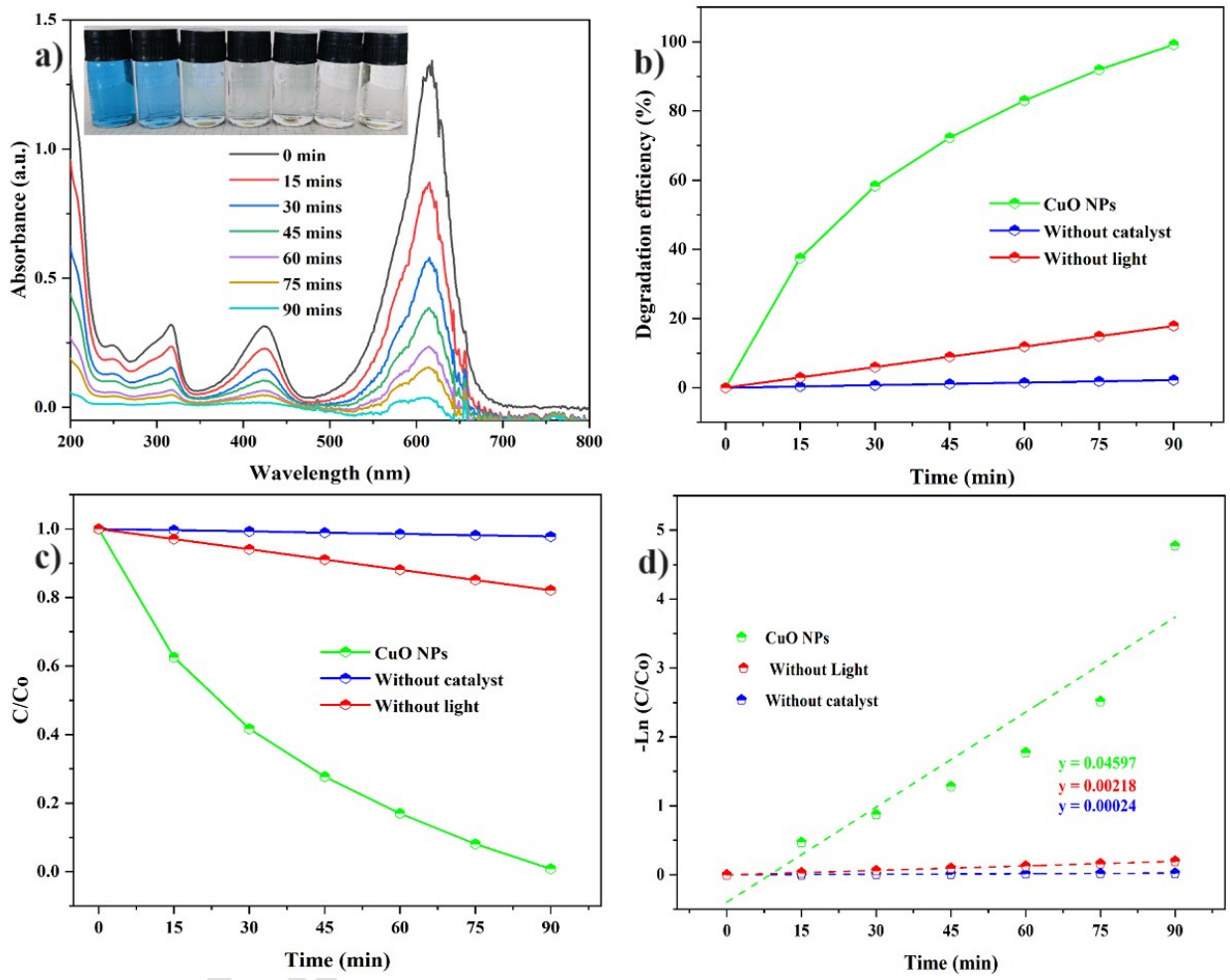

Figure 12. Photocatalytic degradation, efficiency, C_t/C_0 curve concerning time and Pseudo first-order kinetics of the CuO NPs against Malachite Green Dye

Figures 13(a, b) and 14(a, b) demonstrate the photocatalytic potency of the produced CuO NPs against the anionic dyes Reactive Black and Eosin Yellow. As previously stated, the reaction solutions were stirred for 30 minutes in a dark environment to attain homogeneity. Then, the solution was facilitated with sunlight and examined every 15 minutes under UV-Vis spectroscopy to observe the time-dependent degradation of cationic dyes. The characteristic peaks of Reactive Black and Eosin Yellow dyes were 598 nm and 517 nm, respectively (Laohaprapanon *et al.* 2015). The observation was continued for 90 minutes, where the CuO NPs reached the maximum degradation efficacy against those cationic dyes. CuO NPs demonstrated 89.73% and 89.60%

photocatalytic efficacy against Reactive Black and Eosin Yellow, respectively. The same procedures were followed for the cationic dyes to access the self-degradation and light-dependent degradation of dye molecules, as mentioned for the cationic dyes. The self-degradation of the cationic dyes without the catalyst was estimated as 1.85% for the Reactive Black and 22% for Eosin Yellow dyes. The light-dependent catalytic efficacy of the nanomaterials was evaluated as 9.25% for the Reactive black and 9.78% for the Eosin Yellow dyes, respectively.

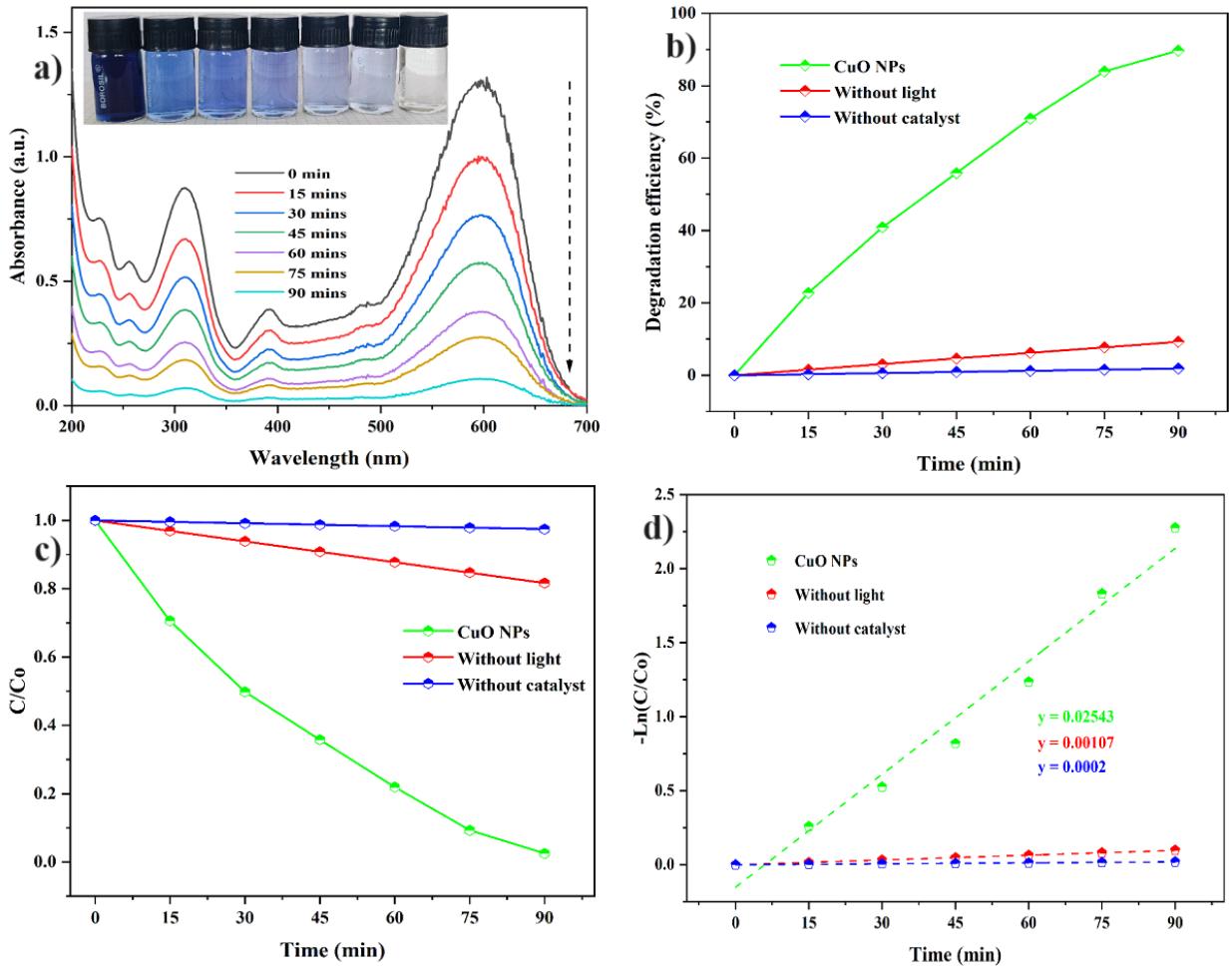

Figure 13. Photocatalytic degradation, efficiency, C_t/C_0 curve concerning time and Pseudo first-order kinetics of the CuO NPs against Reactive Black Dye

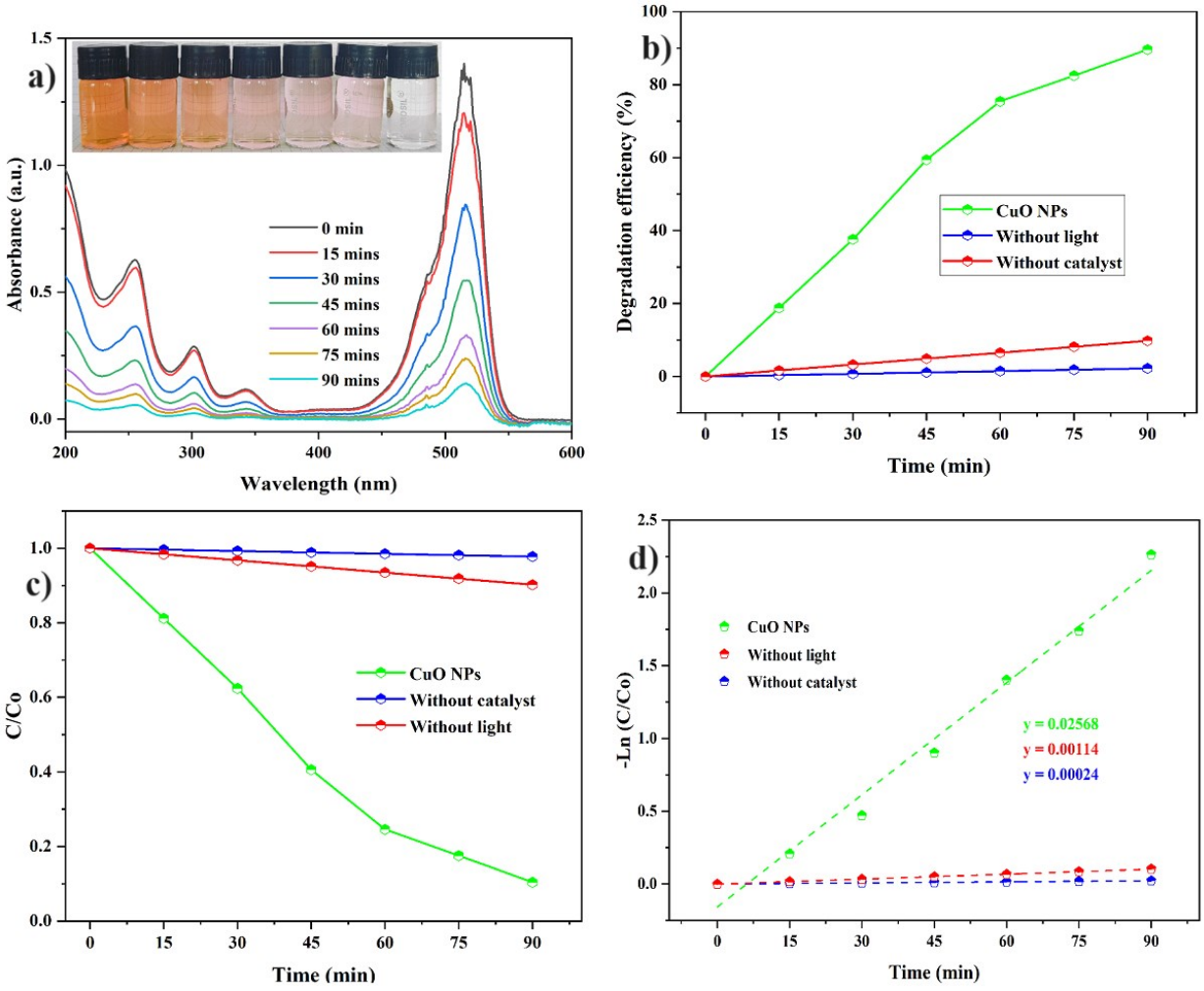

Figure 14. Photocatalytic degradation, efficiency, C_t/C_0 curve concerning time and Pseudo first-order kinetics of the CuO NPs against Eosin Yellow Dye

These data unequivocally exhibited that the green-synthesized CuO NPs were a potent photocatalytic agent. *Nerium oleander* leaf extract was used as a capping and reducing agent, which resulted in the production of an excellent photocatalyst. The controlled particle size and improved surface properties resulted in enhanced surface area that led to the higher interaction between the nanomaterial and organic dye molecules and resulted in the effective degradation of hazardous organic dye molecules. Notably, the constrained band gap of the nanoparticle facilitated the faster electron-hole recombination and active spot production for the decomposition of the organic industrial dye molecules. As mentioned, the prepared CuO NPs were accorded with higher negative zeta potential, directly representing the higher degradation of cationic dyes due to the opposite charge interaction.

Table 3. The following table presents a comparative analysis of the photocatalytic reaction demonstrated by several nanoparticles against different dyes.

Photocatalyst	Dye	Light irradiation	Reaction time (min)	Degradation efficiency (%)	Ref
Ce-SnO_2	Congo Red	UV	120	90	46
	Methylene Blue	UV	120	97	
ZnO	Victoria Blue	Sunlight	40	93	47
CuO	Nile Blue	Sunlight	120	93	48
	Reactive yellow	Sunlight	120	81	
Fe_2O_3	Rhodamine B	Sunlight	40	59	49
Cu NPs	Methylene Blue	Sunlight	85	96	50
MgO	Methylene Blue	UV	120	75	51
ACS-ZnO	Rhodamine B	UV	90	88.75	52
	Methylene Blue	UV	90	93.3	
	Neutral Red	UV	90	86.6	
Ce-SnO_2	Rose Bengal	UV	60	96	53
CuO	Methyl green	Sunlight	120	65.23	54
	Methyl orange	Sunlight	120	65.078	
ZnO	Amaranth dye	UV	75	95.3	55
Ag-CeO_2	Rose Bengal	UV	180	96	56
ZnO	Rhodamine B	UV	120	96.1	57
	Methyl Orange	UV	120	85.7	
La_2O_3	Safranin	UV	120	90.13	58
	Congo red	UV	120	89.66	
Co_3O_4	Methylene Blue	UV	80	93.44	59
	Methyl Orange	UV	80	93.29	
NiO	Safranin	UV	100	92.75	60
	Methyl orange	UV	100	98.02	
La_2O_3–CuO	Safranin	Sun light	135	95.8	61
	Crystal Violet	Sunlight	135	97.05	
La2O3–SnO_2	Safranin	Sun light	135	93.24	62
	Crystal Violet	Sunlight	135	95.28	
CuO	Rhodamine 6G	Sunlight	90	97.48	This
	Malachite Green	Sunlight	90	99.15	work
	Reactive Black	Sunlight	90	89.73	
	Eosin Yellow	Sunlight	90	89.60	

The photocatalytic degradation efficacy results revealed the same by exposing higher efficacy in the degradation cationic dyes, namely Rhodamine 6g and Malachite green. The exceptional photocatalytic activity shown by the CuO nanoparticles that were synthesized is being compared to previous studies, emphasizing the importance of this research. The comparative assessment of the photocatalytic activity is given in Table 3.

3.9 Photocatalytic mechanism and kinetics

Figure 15 exhibited the photocatalytic mechanism of degradation of organic dye molecules against the produced CuO NPs. The CuO nanoparticles in the reaction mixture absorb photons when exposed to light. The absorbed photons in CuO NPs have excited holes (h^+) in the valence band and excited electrons (e^-) in the conduction band, resulting in electron-hole pairs in the CuO lattice. The electrons (e^-) and holes (h^+) participate in redox reactions with water and oxygen molecules in the surrounding environment. Superoxide radicals (O_2^-), hydroxyl radicals ($^{\bullet}OH$), and hydrogen peroxide (H_2O_2) were formed when holes (h^+) oxidize water to generate hydroxyl radical (OH), while electrons (e^-) reduce the oxygen molecules (O_2) to produce superoxide radicals (O_2^-) that leads to the generation of hydrogen peroxide (H_2O_2). The produced superoxide radicals (O_2^-), hydroxyl radicals (OH), and hydrogen peroxide (H_2O_2) are potent oxidizing agents. They attack the organic dye molecules, breaking down their chemical structures. As a result, the dye molecules break down into less toxic, smaller molecules. In the final stages of photodegradation, the dye molecules are further broken down into simpler, non-toxic.

$$\mathbf{CuO\ NPs + Light\ (hv) \rightarrow CuO\ (e^-\ CB) + (h^+\ VB)}$$

$$\mathbf{2e^- + O_2 \rightarrow 2O_2^{\bullet-}}$$

$$\mathbf{2h^+ + 2H_2O \rightarrow 4OH^{\bullet} + O_2}$$

$$\mathbf{OH^{\bullet} + 2H_2O \rightarrow 2H_2O_2}$$

$$\mathbf{CuO\ NPs + dye\ pollutants\ (RMS) \rightarrow degradation\ products}$$

Table 4. Rate Constant of the reactions

Dyes / Conditions	Rhodamine 6G ($x10^{-2}$)	Malachite Green ($x10^{-2}$)	Reactive Black ($x10^{-2}$)	Eosin Yellow ($x10^{-2}$)
With Catalyst and Light	4.026	4.597	2.543	2.568
Without Catalyst	0.0289	0.0251	0.0208	0.025
Without Light	0.225	0.2186	0.1079	0.1144

(CB, VB, and RMS represent the Conduction Band, Valance Band, and Reaction Mixture Solution, respectively).

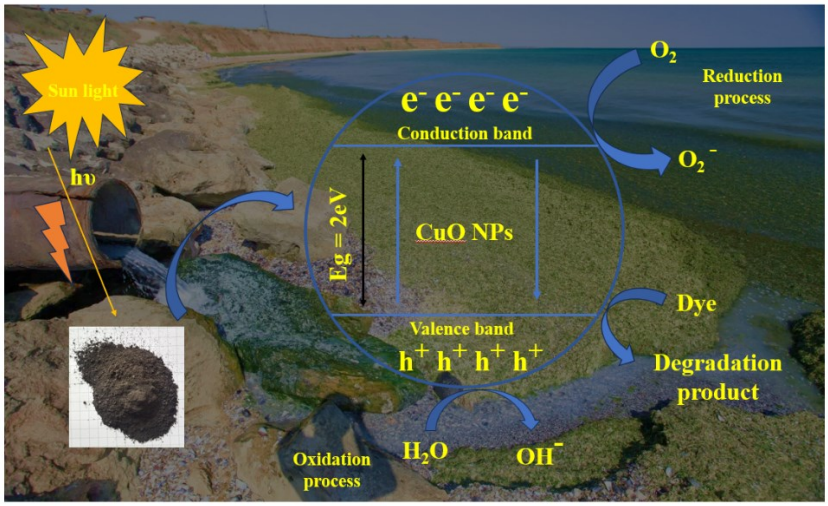

Figure 15. Photocatalytic Mechanism of the CuO NPs.

3.10 Recyclability and Stability

Reusing the same nanoparticles for numerous cycles of photocatalysis allowed researchers to observe the recyclability and stability of the CuO NPs that were created earlier. Figure 16 presents the outcomes that were seen in the experimentation. To evaluate the possibility of the created NPs being used repeatedly in photocatalytic applications, their recyclability and stability were put under the microscope. After the first cycle of photocatalysis was finished, the nanomaterial was collected and centrifuged three times with ethanol and water separately to eradicate any impurities attached to the surface of the nanomaterial. After being dried in a hot air oven, the nanomaterial was utilized for the succeeding cycle of photocatalysis. Similarly, five uninterrupted cycles of photocatalysis were conducted as an experiment to determine the nanomaterial's level of stability. Throughout five cycles, the nanomaterial showed a degradation efficacy of 94.01%, 92.8%, 82.01%, and 84.11% for Rhodamine 6G, Malachite Green, and Reactive Black, respectively. Eosin Yellow showed a degradation efficacy of 84.11%.

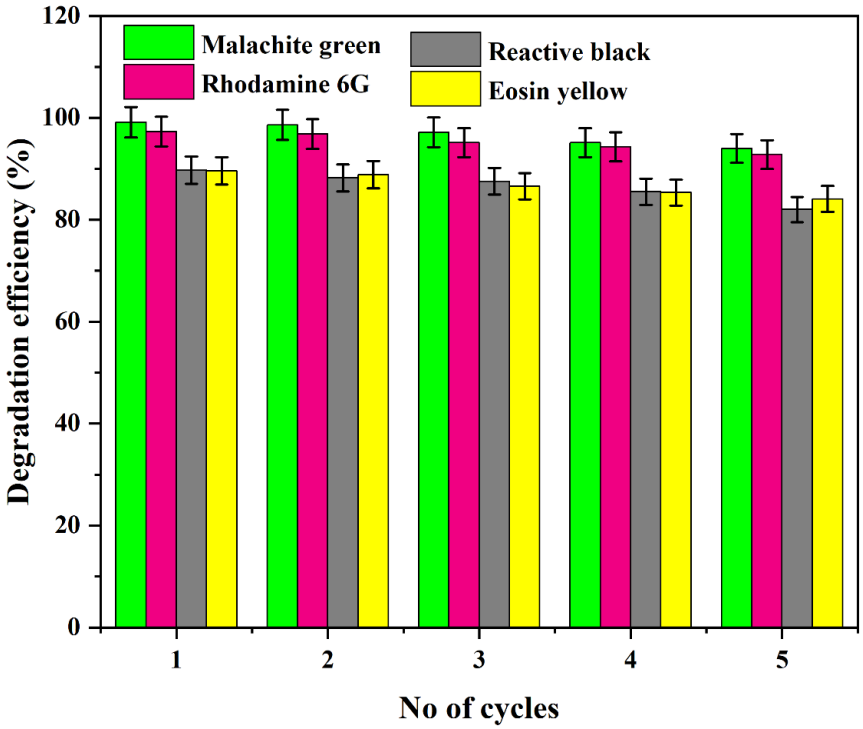

Figure 17. Recyclable Efficacy of the CuO NPs over five cycles.

These results proved the remarkable durability and sustained efficacy of these nanoparticles over numerous cycles of photocatalysis, highlighting the Nerium oleander leaf extract's substantial role in capping and reducing, which contributed to the structural stability of the nanoparticles. The results also demonstrated these nanoparticles' remarkable durability and sustained efficacy over multiple cycles of photocatalysis. Even after numerous cycles of photocatalysis, the structural integrity of the nanoparticles was preserved thanks to the regulated particle size and better surface properties that resulted from this environmentally friendly synthesis approach. These factors occupied a significant role in protecting the structural integrity of the nanoparticles. Using plant extract proved highly efficient in preventing agglomeration and ensuring that the nanoparticles kept their photocatalytic activity for many cycles. The outstanding recyclability and stability of the created CuO NPs were confirmed by their efficiency in degrading organic dye molecules, which was maintained at a high level for five cycles in a row without experiencing a slight decline in that efficiency. Figures 12(c), 13(c), and 14(c) display the time-dependent degradation of dye molecules, specifically for the Rhodamine 6G, Malachite Green, Reactive Black, and Eosin Yellow dye molecules. In addition to that, the rate constant was depicted in Figures 12(d), 13(d), 14(d), and 15(d), respectively. Pseudo-first-order kinetics, in which the concentration of its

reactants determines the reaction rate, is the type of kinetics the reactions typically follow. Consequently, the pseudo-first-order kinetic equation is utilized to compute the photocatalytic degradation propensity of the dye catalyst. To determine the rate of organic dye degradation produced by the CuO NPs, the first-order kinetic equation (4) was utilized.

$$\ln(^{C_t}/_{C_0}) = kt \qquad (4)$$

Where, C_t is the representation of the concentration of the reactant at time t, C_0 is the representation of the initial concentration of the reactant, k is the representation of the rate constant for the reaction, and t is the representation of the reaction time. The rate constant of the reactions for the anionic and cationic dyes was estimated and tabulated in Table (3). Additionally, the rate constant of the reactions that were experimented with to access the self-degradation and light-dependent degradation of the organic dye molecules were included in Table (3).

4. Conclusion

In conclusion, the CuO NPs were prepared using *Nerium oleander* leaf extract as the natural reducing and capping agent. This allowed for the synthesis to be considered environmentally friendly. Nanoparticles with increased catalytic activity have been produced using this ecologically friendly technology, which also demonstrated the significant potential of plant-based reducing agents in fine-tuning the physicochemical features of nanoparticles. The XRD and the particle size analyzer both showed that the particle size had been significantly reduced, and surface-oriented investigations demonstrated that the CuO NPs had better surface properties. For the degradation of various industrial dyes, like Rhodamine 6G, Eosin Yellow, Reactive Black, and Malachite Green, the physiochemically modified CuO NPs have proven to be a very effective and eco-friendly technique. Amazingly, the natural phytochemicals in Nerium oleander leaves performed exceptionally well as both capping and reducing agents, which resulted in remarkable stability. The CuO nanoparticles proved their durability during many cycles of photocatalysis, which resulted in the successful degradation of the industrial colors. This study highlights the possibilities of environmentally friendly synthesis in materials science. It sheds light on the essential part that reducing agents derived from plants play in expanding the field of environmentally friendly nanomaterials for wastewater treatment and environmental remediation.

References

Alaton I.A. and Balcioglu I.A. (2001). Photochemical and Heterogeneous Photocatalytic Degradation of Waste Vinylsulphone Dyes: A Case Study with Hydrolyzed Reactive Black 5. *Journal of Photochemistry and Photobiology A,* **141,** 247–254.

Al-Tohamy R., Ali S.S., Li F., Okasha K.M., Mahmoud Y.A.G., Elsamahy T., Jiao H., Fu Y. and Sun J. (2022). A Critical Review on the Treatment of Dye-Containing Wastewater: Ecotoxicological and Health Concerns of Textile Dyes and Possible Remediation Approaches for Environmental Safety. *Ecotoxicology and Environmental Safety,* **231,** 113160.

Berradi M., Hsissou R., Khudhair M., Assouag M., Cherkaoui O., Bachiri A. and Harfi A. (2019). Textile Finishing Dyes and Their Impact on Aquatic Environs. *Heliyon,* **5,** e02711.

Bilal M., Rasheed T., Iqbal H.M.N., Hu H., Wang W. and Zhang X. (2018). Toxicological Assessment and UV/TiO_2-Based Induced Degradation Profile of Reactive Black 5 Dye. *Environmental Management,* **61,** 171–180.

Chen C.C., Lu C.S., Chung Y.C. and Jan J.L. (2007). UV Light Induced Photodegradation of Malachite Green on TiO_2 Nanoparticles. *Journal of Hazardous Materials,* **141,** 520–528.

Eskizeybek V., Sarı F., Gulce H., Gülce A. and Avc A. (2012). Preparation of the New polyaniline/ZnO Nanocomposite and Its Photocatalytic Activity for Degradation of Methylene Blue and Malachite Green Dyes under UV and Natural Sun Lights Irradiations. *Applied Catalysis B.* **119,** 197–206.

Ghazzal M.N., Kebaili H., Joseph M., Debecker D.P., Eloy P., Coninck J. and Gaigneaux E.M. (2012). Photocatalytic Degradation of Rhodamine 6G on Mesoporous Titania Films: Combined Effect of Texture and Dye Aggregation Forms. *Applied Catalysis B,* **115-116,** 276–284.

Kumari H., Sonia S., Ranga R., Chahal S., Devi S., Sharma S. and Kumar S. (2023). A Review on Photocatalysis Used for Wastewater Treatment: Dye Degradation. *Water, Air, & Soil Pollution,* **234,** 0349.

Kuspanov Z., Bakbolat B., Baimenov A., Issadykov A., Yeleuov M. and Daulbayev C. (2023). Photocatalysts for a Sustainable Future: Innovations in Large-Scale Environmental and Energy Applications. *Science of The Total Environment,* **885,** 163914.

Laohaprapanon S., Matahum J., Tayo L. and You S.J. (2015). Photodegradation of Reactive Black 5 in a ZnO/UV Slurry Membrane Reactor. *Journal of the Taiwan Institute of Chemical Engineers*, **49,** 136-141.

Lucas M.S. and Peres J.A. (2006). Decolorization of the Azo Dye Reactive Black 5 by Fenton and Photo-Fenton Oxidation. *Dyes and Pigments*, **71,** 236–244.

Luna I.Z., Hilary L.N., Chowdhury A.M.S., Gafur M.A., Khan N. and Khan R.A. (2015). Preparation and Characterization of Copper Oxide Nanoparticles Synthesized via Chemical Precipitation Method. *OALib Journal***, 02,** 1–8.

Pakhale V.D. and Gogate P.R. (2021). Removal of Rhodamine 6G from Industrial Wastewater Using Combination Approach of Adsorption Followed by Sonication. *Arabian Journal for Science and Engineering,* **46,** 6473–6484.

Renuga D., Jeyasundari J., Shakthi A.S. and Brightson Y. (2020). Synthesis and Characterization of Copper Oxide Nanoparticles Using Brassica Oleracea Var. Italic Extract for Its Antifungal Application. *Materials Research Express,* **7,** 045007.

Roisnel T. and Rodríquez-Carvajal J. (2001). WinPLOTR: a windows tool for powder diffraction pattern analysis. *Materials Science Forum,* **378,** 118-123.

Sadollahkhani A., Hussain Z., Elhag S., Nur O. and Willander M. (2014). Photocatalytic Properties of Different Morphologies of CuO for the Degradation of Congo Red Organic Dye. *Ceramics International,* **40,** 11311–11317.

Sebeia N., Jabli M. and Ghith A. (2019), Biological Synthesis of Copper Nanoparticles, Using Nerium Oleander Leaves Extract: Characterization and Study of Their Interaction with Organic Dyes. *Inorganic Chemistry Communications,* **105,** 36–46.

Shirmardi M., Mahvi A.H., Hashemzadeh B., Naeimabadi A., Hassani G. and Niri M.V. (2013). The Adsorption of Malachite Green (MG) as a Cationic Dye onto Functionalized Multi Walled Carbon Nanotubes. *Korean Journal of Chemical Engineering,* **30,** 1603–1608.

Singh D., Jain D., Rajpurohit D., Jat G., Kushwaha H.S., Singh A., Mohanty S.R., Al-Sadoon M.K., Zaman W. and Upadhyay S.K. (2023). Acteria Assisted Green Synthesis of Copper Oxide Nanoparticles and Their Potential Applications as Antimicrobial Agents and Plant Growth Stimulants. *Frontiers in Chemistry*, **11,** 1154128.

Singh J., Kumar V., Kim K.H. and Rawat M. (2019). Biogenic Synthesis of Copper Oxide Nanoparticles Using Plant Extract and Its Prodigious Potential for Photocatalytic Degradation of Dyes. *Environmental Research,* **177,** 108569.

Sorbiun M., Shayegan E., Ramazani A. and Taghavi S. (2018). Green Synthesis of Zinc Oxide and Copper Oxide Nanoparticles Using Aqueous Extract of Oak Fruit Hull (Jaft) and Comparing Their Photocatalytic Degradation of Basic Violet 3. *International Journal of Environmental Research,* **12,** 29–37.

Udayabhanu P.C., Kumar M.A., Suresh D., Lingaraju K., Rajanaika H., Nagabhushana H. and Sharma S.C. (2015). Tinospora Cordifolia Mediated Facile Green Synthesis of Cupric Oxide Nanoparticles and Their Photocatalytic, Antioxidant and Antibacterial Properties. *Materials Science in Semiconductor Processing,* **33,** 81–88.